Structural Determinants for the Selectivity of the Positive KCa3.1 Gating Modulator 5-Methylnaphtho[2,1-*d*]oxazol-2-amine (SKA-121)

Brandon M. Brown, Heesung Shim, Miao Zhang, Vladimir Yarov-Yarovoy, Heike Wulff

Department of Pharmacology (B.M.B., H.S., H.W.), Department of Physiology and Membrane Biology (V. Y.-Y.), School of Medicine, and Department of Chemistry (H.S.), University of California, Davis, California, USA; Department of Biomedical and Pharmaceutical Sciences (M.Z), Chapman University School of Pharmacy, Irvine, California, USA.

Running Title: Molecular Model of the SKA-121 Binding Site

Address correspondence to:

Heike Wulff, Department of Pharmacology, Genome and Biomedical Sciences Facility, Room

3502, 451 Health Sciences Drive, University of California, Davis, Davis, CA 95616; phone: 530-

754-6136; email: hwulff@ucdavis.edu

Number of Text Pages: 34

Number of Tables: 0

Number of Figures: 7

Number of References: 55

Number of Words in the Abstract: 250

Number of Words in the Introduction: 752

Number of Words in the Discussion: 1,309

Nonstandard abbreviations used: CaM, calmodulin; CaM-BD, calmodulin binding domain;

DMSO, dimethyl sulfoxide; EBIO, 1-ethylbenzimidazolin-2-one; HEK, human embryonic kidney;

K_{Ca}, Ca^{2+}-activated K^+ channel; $K_{Ca}3.1$, intermediate-conductance Ca^{2+}-activated K^+ channel;

K_V, voltage-gated K^+ channel; NS309, 6,7-dichloro-1*H*-indole-2,3-dione 3-oxime; SK, small-

conductance K_{Ca} channel; SKA-31, naphtho[1,2-*d*]thiazol-2-ylamine; SKA-111, 5-

methylnaphtho[1,2-*d*]thiazol-2-amine; SKA-121, 5-methylnaphtho[2,1-*d*]oxazol-2-amine.

Abstract

Intermediate-conductance ($K_{Ca}3.1$) and small-conductance ($K_{Ca}2$) calcium-activated K^+ channels are gated by calcium binding to calmodulin (CaM) molecules associated with the calmodulin binding domain (CaM-BD) of these channels. The existing K_{Ca} activators like SKA-31, NS309 and EBIO activate both channel types with similar potencies. In a previous chemistry effort we optimizes the benzothiazole pharmacophore of SKA-31 towards $K_{Ca}3.1$ selectivity and identified SKA-121 (5-methylnaphtho[2,1-*d*]oxazol-2-amine), which exhibits 40-fold selectivity for $K_{Ca}3.1$ over $K_{Ca}2.3$. In order to understand why introduction of a single CH_3 group in 5-position of the benzothiazole/oxazol system could achieve such a gain in selectivity for $K_{Ca}3.1$ over $K_{Ca}2.3$ we first localized the binding site of the benzothiazoles/oxazoles to the CaM-BD/CaM interface and then used the RosettaLigand computational modeling software to generate models of the $K_{Ca}3.1$ and $K_{Ca}2.3$ CaM-BD/CaM complexes with SKA-121. Based on a combination of mutagenesis and structural modeling we suggest that all benzothiazoles/oxazoles-type K_{Ca} activators bind relatively "deep" in the CaM-BD/CaM interface and hydrogen-bond with E54 on CaM. In $K_{Ca}3.1$ SKA-121 forms an additional hydrogen-bond network with R362. NS309 in contrast sits more "forward" and directly hydrogen-bonds with R362 in $K_{Ca}3.1$. Mutating R362 to serine, the corresponding residue in $K_{Ca}2.3$ reduces the potency of SKA-121 by 7-fold suggesting that R362 is responsible for the generally greater potency of K_{Ca} activators on $K_{Ca}3.1$. The increase in SKA-121's $K_{Ca}3.1$ selectivity compared with its parent SKA-31 seems to be due to better overall shape complementarity and hydrophobic interactions with S372, M368 on $K_{Ca}3.1$ and M72 on CaM at the $K_{Ca}3.1$-CaM-BD/CaM interface.

Introduction

Small- and intermediate-conductance calcium-activated potassium channels (K_{Ca}) are gated by the binding of calcium to calmodulin (CaM), which is constitutively associated with the calmodulin binding domain (CaM-BD) on the C-terminus of these voltage-independent channels. There are four channels in the so-called $K_{Ca}2/3$ group: the small-conductance $K_{Ca}2.1$, $K_{Ca}2.2$, and $K_{Ca}2.3$, known collectively as SK channels, and the intermediate-conductance $K_{Ca}3.1$ channel, also known as IK (Wei et al., 2005). $K_{Ca}2/3$ channels share a similar over-all structure with the voltage-gated potassium channel (K_V) family. The channels are tetramers consisting of four six-transmembrane domains with the N- and C- termini located on the cytoplasmic side of the membrane. $K_{Ca}2$ and $K_{Ca}3.1$ channels have the same Ca^{2+}/calmodulin mediated gating mechanism (Fanger et al., 1999; Xia et al., 1998), but differ in their conductance, with $K_{Ca}2$ channels having a single channel conductance of ~2 pS and $K_{Ca}3.1$ having a single channel conductance of 11 pS at physiological potassium concentrations (Wei et al., 2005). While $K_{Ca}2$ channels are primarily expressed in the nervous system (Adelman et al., 2012), $K_{Ca}3.1$ is predominantly found in peripheral tissues (Wulff and Castle, 2010). In both cases K_{Ca} channel activation hyperpolarizes the cell membrane inducing different physiological effects depending on the location of expression. For example, in immune cells $K_{Ca}3.1$ channels regulate calcium influx and cellular activation (Feske et al., 2015); in the vascular endothelium both $K_{Ca}3.1$ and $K_{Ca}2.3$ contribute to controlling vascular tone (Busse et al., 2002); while in neurons $K_{Ca}2$ channels mediate afterhyperpolarization, regulate firing frequency and contribute to learning and memory (Adelman et al., 2012). Pharmacologic activation of K_{Ca} channels therefore seems attractive for the treatment of neurological and cardiovascular diseases (Christophersen and Wulff, 2015; Lam et al., 2013). Specifically, $K_{Ca}2$ channel activation has been proposed for reducing neuronal excitability in epilepsy and ataxia, while $K_{Ca}3.1$ activation could potentially provide a novel therapeutic strategy to treat hypertension.

While the therapeutic potential of activating $K_{Ca}2/3$ channels is clear, it has been a challenge to develop subtype selective compounds. The majority of $K_{Ca}2/3$ channel activators suffer from a lack of selectivity, displaying only a modest 5- to 10-fold selectivity for $K_{Ca}3.1$. In 1996 the first compound identified to activate K_{Ca} channels was 1-EBIO or simply EBIO (Devor et al., 1996). EBIO has been reported to activate $K_{Ca}3.1$ with EC_{50} values ranging from 28 to 210 μM (Jensen et al., 1998; Pedarzani et al., 2001; Singh et al., 2001; Syme et al., 2000), $K_{Ca}2.1$ at 630 μM, $K_{Ca}2.2$ at 500 μM to 1 mM, and $K_{Ca}2.3$ at 170 μM to 1 mM (Cao et al., 2001; Hougaard et al., 2007; Lappin et al., 2005; Pedarzani et al., 2001). Another widely used $K_{Ca}2/3$ activator is SKA-31, a compound which was developed in our laboratory using the neuroprotectant riluzole as a structural template (Sankaranarayanan et al., 2009). While SKA-31 is more potent than EBIO and activates $K_{Ca}3.1$ with an EC_{50} of 260 nM and $K_{Ca}2$ channels with EC_{50}s of 1.9 and 2.9 μM, it also still suffers from a lack of selectivity. Through further derivatization of SKA-31 we more recently identified SKA-121, the first selective $K_{Ca}3.1$ activator (Coleman et al., 2014). SKA-121 displays 40-fold selectivity for $K_{Ca}3.1$ (EC_{50} = 110 nM) over $K_{Ca}2.3$ (EC_{50} = 4.4 μM) and slightly greater selectivity over $K_{Ca}2.2$ and $K_{Ca}2.1$. Interestingly, this gain in selectivity for $K_{Ca}3.1$ over $K_{Ca}2.3$ was achieved by a very minor structural change, addition of a methyl group in 5-position of the napthothiazole or the related napthooxazole ring system. We were very intrigued to observe this "magic methyl effect", meaning that the installation of a single methyl group in the "right" location on a chemical scaffold can result in a significant activity shift (Leung et al., 2012) and therefore wanted to identify the binding site of the napthothiazole/oxazole-type K_{Ca} activators and, if possible, understand this selectivity at the molecular level.

Using the recently determined X-ray crystal structures of the $K_{Ca}2.2$ CaM-BD in complex with CaM and containing the K_{Ca} activators EBIO (Zhang et al., 2012) or NS309 (Zhang et al., 2013) we here employed a combination of RosettaLigand molecular modeling and site directed mutagenesis to generate homology models of the $K_{Ca}3.1$ and $K_{Ca}2.3$ CaM-BD/CaM complex

5

containing SKA-121, SKA-111, SKA-31, EBIO and NS309 in the interface. $K_{Ca}3.1$ selectivity

seems to be due to the presence of R362, a residue which is at the center of an extensive

hydrogen bond network stabilizing SKA-121 in $K_{Ca}3.1$. If R362 in $K_{Ca}3.1$ is replaced by a serine

like in the $K_{Ca}3.1$-R362S mutant or in $K_{Ca}2.3$ the hydrogen bond network is not present.

Material and Methods

Chemicals and Reagents. SKA-121 and SKA-31 were synthesized in the Wulff laboratory as previously described and characterized by ^{1}H and ^{13}C-NMR for identity and by UPLC/MS for purity (Coleman et al., 2014; Sankaranarayanan et al., 2009). EBIO and NS309 were purchased from Sigma (St. Louis, MO). Standard laboratory chemicals were purchased from commercial vendors and were of the purest available grade. K_{Ca} activator stocks (1 or 10 mM) were prepared in dry DMSO and drug dilutions for all electrophysiology experiments were always freshly prepared during the experiment to avoid any potential precipitation of compounds. The final DMSO concentration typically was around 0.1% and never exceeded 1%.

Molecular Biology. The cloning of human K_{Ca}3.1 (#AF033021) and K_{Ca}2.3 (#AJ251016) has been reported in the late 1990s (Chandy et al., 1998; Logsdon et al., 1997). Both channel genes were subcloned in-frame downstream to green fluorescent protein in the pEGFP-C1 expression vector (CLONTECH) (Wulff et al., 2001). All clones were verified by sequencing. Mutations were introduced using the QuikChange site directed mutagenesis kit (Stratagene, La Jolla, CA) and were verified by fluorescence sequencing. For amino acid numbering for KCa3.1 we used the gene: Homo sapiens potassium channel, calcium activated intermediate/small conductance subfamily N alpha, member 4 (KCNN4). NCBI Reference Sequence: NP_002241.1. For amino acid numbering for K_{Ca}2.3 we used the gene: Homo sapiens potassium channel, calcium activated intermediate/small conductance subfamily N alpha, member 3 (KCNN3), transcript variant 1, mRNA. NCBI Reference Sequence: NM_002249.5. This corresponds to the Q14 variant of K_{Ca}2.3.

Electrophysiology. All experiments were performed in either the inside-out or the whole-cell configuration of the patch-clamp technique on transiently transfected COS-7 cells. COS-7 cells

were purchased from American Type Culture Collection (ATCC, Manassas, VA) and cultured in

DMEM supplemented with 10% fetal calf serum. WT and mutant $K_{Ca}3.1$ and $K_{Ca}2.3$ channel

constructs were transfected using FuGENE® 6 transfection reagent (Promega, Madison, WI) in

Opti-MEM® reduced serum medium (Life Technologies, Benicia, CA). Cells were cultured in 6-

well plates for 48 h and then detached by TrypLE™ Express (Gibco, Grand Island, NY) and

plated on coverslips for 30 min to 1 h for whole-cell recordings. For inside-out recordings cells

were plated 2-3 h before the experiments to attach them more firmly. Coverslips were placed in

a 15-μl recording chamber mounted on an inverted microscope (Olympus XI-70 equipped with

fluorescence burner and filters; Olympus, Tokyo, Japan), and only clearly green fluorescent

cells were patch-clamped. To reduce contaminating currents from native chloride channels in

COS-7 cells, solutions contained aspartate instead of chloride. For whole-cell experiments the

extracellular solution contained 160 mM Na^+-aspartate, 4.5 mM KCl, 2 mM $CaCl_2$, 1 mM $MgCl_2$

and 10 mM HEPES (pH 7.4, 300 mOsm). Solutions on the intracellular side contained 160 mM

K^+-aspartate, 10 mM HEPES, 10 mM EGTA, 2.31 mM $MgCl_2$ and 5.96 mM or 7.2 mM $CaCl_2$ for

a calculated free Ca^{2+} concentrations of 250 or 500 nM (pH 7.2, 290 mOsm). For inside-out

experiments in symmetrical K^+ the extracellular solution contained 160 mM K^+-aspartate, 10 mM

HEPES, 1 mM $MgCl_2$, and 2 mM $CaCl_2$ (pH 7.4, 300 mOsm). Intracellular solutions contained

160 mM K^+-aspartate, 10 mM HEPES, 10 mM EGTA, 2.31 mM $MgCl_2$ and varying amounts of

$CaCl_2$ for calculated free Ca^{2+} concentrations of 0.05, 0.1, 0.25, 0.5, 1, 10, 30 µM (pH 7.2, 300

mOsm). Free Ca^{2+} concentrations were calculated using the 7/3/2009 online version of

MaxChelator   (http://maxchelator.stanford.edu/webmaxc/webmaxcS.htm)   assuming   a

temperature of 25°C, a pH of 7.2, and an ionic strength of 160 mM. Patch pipettes were pulled

from soda lime glass (micro-hematocrit tubes; Kimble Chase, Rochester, NY) and had

resistances of 1.5 to 3 MΩ when submerged. Experiments were controlled with a HEKA EPC-10

amplifier and Pulse software (HEKA, Lambrecht/Pfalz, Germany). In whole-cell experiments,

8

cells were clamped to a holding potential of -80 mV, and K_{Ca} currents were elicited by 200-ms

voltage ramps from -120 to +40 mV applied every 10 s. In inside-out experiments cells were

clamped to a holding potential of -80 mV, and K_{Ca} currents were elicited by 200-ms voltage

ramps from -80 to +80 mV applied every 5 s. Data analysis, fitting, and plotting were performed

with IGOR-Pro (Wavemetrics, Lake Oswego, OR) or Origin 9 (OriginLab Corporation,

Northampton, MA).

Calcium Sensitivity Testing: In order to assess whether specific mutations affected Ca^{2+}-

sensitivity, mutant channels were first patched with an intracellular solution containing 3 μM of

free Ca^{2+}. If the mutant did not display currents with amplitudes in the nA range under these

conditions, the mutant was deemed to have altered Ca^{2+} sensitivity and was excluded from

subsequent experiments investigating sensitivity to SKA-121.

Homology Modeling. We generated preliminary models of the $K_{Ca}3.1$ channel C-terminal CaM-

binding domain in complex with CaM using Rosetta computational modeling software (Mandell

et al., 2009; Rohl et al., 2004; Wang et al., 2007; Yarov-Yarovoy et al., 2006) and an x-ray

structure of the $K_{Ca}2.2$ channel CaM-binding domain in complex with CaM and NS309 (Zhang et

al., 2013)(pdb id: 4J9Z). Due to significant sequence differences between $K_{Ca}3.1$ and $K_{Ca}2$

channels in the loop between the two helices forming the CaM-binding domain, we predicted the

structure of this region *de novo* using Rosetta cyclic coordinate descent (CCD) and kinematic

(KIC) closure loop modeling methods developed to model loop structures with sub-angstrom

accuracy (Mandell et al., 2009; Wang et al., 2007). After performing several rounds of CCD and

KIC loop modeling with at least 10,000 models generated during each round, models were

ranked based on total Rosetta energy (Rohl et al., 2004). Using a root mean square deviation

threshold that placed 1-2 percent of all models in at least one of the largest clusters ten percent

of the lowest energy models were clustered (Bonneau et al., 2002). Models representing

centers of the top 20 clusters (early rounds) and/or the best 10 models by total energy (later rounds) were used as input for the next round of loop modeling. Potential differences in backbone and side chain conformations of $K_{Ca}3.1$ compared to the $K_{Ca}2.2$ structure template were explored using Rosetta's full atom relax protocol (Barth et al., 2007; Rohl et al., 2004). Selection of the best $K_{Ca}3.1$ channel CaM-binding domain in complex with CaM models was guided by clustering of the lowest energy models to generate the most frequently sampled ensembles of models (Bonneau et al., 2002). A Rosetta model of the $K_{Ca}2.3$ channel C-terminal CaM-binding domain in complex with CaM was generated using the same procedure.

Ligand Docking. Ligand docking was performed using the Rosetta-Ligand method (RosettaLigand application from Rosetta program suite version 3.7) which progresses in three stages from low-resolution conformational sampling and scoring to full atom optimization using the all-atom energy function (Davis and Baker, 2009; Davis et al., 2009; Meiler and Baker, 2006). In the first, low-resolution stage, the ligand was placed randomly within the binding site and its "center of mass" was constrained to move within a 10 Å diameter sphere. Ligand conformers were generated using Open Eye OMEGA software version 2.5.1.4 (OpenEye Scientific Software) (Hawkins and Nicholls, 2012; Hawkins et al., 2010; OEChem) and were then randomly rotated as a rigid body and scored for shape compatibility with the protein. The best-scoring models were filtered by RMSD to eliminate near-duplicates and one of the remaining models was selected at random to continue to the next stage. The second, high-resolution stage employed the Monte Carlo minimization protocol in which the ligand position and orientation were randomly perturbed by a small deviation (0.1 Å and 3°); receptor side chains were repacked using a rotamer library; the ligand position, orientation, and torsions and protein side-chain torsions were simultaneously optimized using quasi-Newton minimization and the end result was accepted or rejected based on the Metropolis criterion. Scoring used the full-atom Rosetta energy function with softened van der Waals repulsion. The side-chain rotamers

were searched simultaneously during "full repack" cycles and one at a time in the "rotamer trials" cycles. The full repack makes ~10^6 random rotamer substitutions at random positions and accepted or rejected each on the Metropolis criterion. Rotamer trials chose the single best rotamer at a random position in the context of the current state of the rest of the system, with the positions visited once each in random order. The ligand was treated as a single residue and its input conformers served as rotamers during this stage. During the energy minimization step, the finely sampled rotamer library and soft-repulsive energy function allow access to off-rotamer conformations. The third and final stage was a more stringent gradient-based minimization of the ligand position, orientation, and torsions and the receptor torsions for both side chains and backbone. Scoring used the same Rosetta energy function, but with a hard-repulsive van der Waals potential, which created a more rugged energy landscape that was better at discriminating native from non-native binding modes. A total of 10,000 models were generated for each docking trial using an UC Davis cluster system (Cabernet). To identify the best model, the models were first screened with total energy score (Rosetta energy term: score) and the top 1,000 models with the lowest total energy score were selected. They were further scored with the binding energy between ligand and channel. Binding energy (interface_delta_X) was calculated as the difference in total energy between the complex with the ligand bound and the complex with the ligand separated from the binding site. The top 10 models with the lowest binding energy were identified as the candidates that exhibited good structural convergence. All the molecular graphics of ligand and K_{Ca} channel C-terminal CaM-binding domain in complex with CaM were rendered using the UCSF Chimera software (Pettersen et al., 2004).

Protein Data Bank (pdb) format files of the Rosetta models of the K_{Ca}3.1 and K_{Ca}2.3 channel CaM-BD/CaM with and without SKA-121 in the interface are provided in the Data Supplement; pdb files of all other models are available upon request.

Results

The Positive Gating Modulator SKA-121 Increases the Open-Probability (PO) of $K_{Ca}3.1$ and $K_{Ca}2.3$. Positive gating modulators of K_{Ca} channels like EBIO and NS309 increase channel open probability (PO) at a given intracellular Ca^{2+} concentration thus "potentiating" the current and resulting in a leftward shift of the apparent Ca^{2+} concentration-response curve (Li et al., 2009; Pedarzani et al., 2001; Zhang et al., 2013). We previously showed that SKA-121 has similar potentiating effects on $K_{Ca}3.1$ by increasing PO in a calcium-dependent manner and displays ~40-fold selectivity for $K_{Ca}3.1$ over $K_{Ca}2.3$ (Coleman et al., 2014). Accordingly, a concentration of 1 µM SKA-121 maximally activates $K_{Ca}3.1$ while only minimally activating $K_{Ca}2.3$ (Fig. 1A and 1B). What was not investigated previously was whether SKA-121 also increased the open channel probability and shifts the Ca^{2+} concentration response curve of $K_{Ca}2$ channels. We therefore performed inside-out experiments on COS-7 cells stably expressing human $K_{Ca}2.3$, varied the intracellular $[Ca^{2+}]_i$ concentration and found free calcium EC_{50}s of 1.19 µM in the absence of SKA-121 and of 0.41 µM in the presence of 20 µM SKA-121 (Fig. 1D). Interestingly, in addition to a clear left shift of the Ca^{2+} concentration activation response curve of $K_{Ca}2.3$, there also was an increase in maximal effect even at free Ca^{2+} concentrations of 10 and 30 µM. This was somewhat surprising, since, unlike $K_{Ca}3.1$ channels, which have a relatively low Ca^{2+}-dependent $P_o(max)$ (Gerlach et al., 2001; Jones et al., 2007), $K_{Ca}2$ channels are supposedly fully open at saturating $[Ca_{2+}]_i$ concentrations. The Ca^{2+} concentration activation response curve for $K_{Ca}3.1$ is shown for comparison (Fig. 1C). The free calcium EC_{50} for $K_{Ca}3.1$ was found to be 0.59 µM, and shifted to 0.42 µM in the presence of 500 nM SKA-121 with a simultaneously 2-fold increase in the maximally achievable current (Fig. 1C). These data suggest that SKA-121, while more potent on $K_{Ca}3.1$ and inducing a larger increase in PO under comparable recording conditions, acts as a positive gating modulator that "potentiates" current in a Ca^{2+} dependent manner on both $K_{Ca}3.1$ and $K_{Ca}2.3$.

The CaM-BD is the Functional Binding Site for K_{Ca} Channel Activators. Based on their similar mechanism of action and the overall structural similarity between napthothiazole/oxazole-type K_{Ca} activators like SKA-31 and SKA-121 and benzimidazole-type activators like EBIO and NS309, we suspected that SKA-121 is binding at the interface between calmodulin (CaM) and the calmodulin-binding domain (CaM-BD). Zhang et al. soaked EBIO into the protein crystal of CaM bound to the CaM-BD of K_{Ca}2.2 (Zhang et al., 2012). In a subsequent study the same group obtained a co-crystal of the CaM-BD/CaM with NS309 (Zhang et al., 2013). Both molecules reside in a pocket formed at the interface between CaM-BD/CaM and the more potent NS309 seems to facilitate channel gating by affecting the conformation of an intrinsically disordered stretch of nine amino acids, which connects transmembrane segment S6 to the CaM-BD (Zhang et al., 2013).

Since the sequences of K_{Ca}2.2 and K_{Ca}2.3 in the CaM-BD are similar to each other but differ from K_{Ca}3.1 (Fig. 2A), we performed site-directed mutagenesis in order to determine whether the CaM-BD/CaM interface identified in the Zhang work also represented the binding site of the napthothiazole/oxazole-type K_{Ca} activators like SKA-31 and SKA-121. As a first step we created the K_{Ca}2.3 mutation A625I and the double mutation A625V/L628M because the corresponding K_{Ca}2.2 mutations (A477I and A477V/L480M) had been shown by Zhang *et al.* to modify EBIO activity. While the double mutant, which makes K_{Ca}2.2 more K_{Ca}3.1-"like" had been reported to be more EBIO sensitive, the single mutant had made K_{Ca}2.2 less sensitive to EBIO (Zhang et al., 2012). For K_{Ca}2.3 the corresponding mutants both decreased EBIO (not shown) and SKA-31 sensitivity (Fig. 2B) suggesting that the CaM-BD/CaM interface is also the binding site for the napthothiazole/oxazole-type K_{Ca} activators but that there are subtle differences between the individual K_{Ca} channels and/or the exact orientation of the different activators in the interface pocket.

We next switched from the proto-type compound SKA-31 to the $K_{Ca}3.1$ selective compound SKA-121 and tested how mutations of the corresponding positions, V365 and M368 in $K_{Ca}3.1$, would affect SKA-121 potency. We created four mutants: V365A, V365F, M368A, and M368L. The mutant V365F was generated to incorporate a bulky amino acid into the binding pocket to potentially disturb SKA-121 binding and M368A was created to remove potential SKA-121 interaction points. All four mutations exhibited normal Ca^{2+} sensitivity and the responses to 500 nM SKA-121 are summarized in Figure 2C. We had expected that the V365A and V365F mutants would be less sensitive to SKA-121 than the WT channel. However, V365A, V365F and M368A were not statistically different in their responses to 500 nM SKA-121 (29.20 ± 18.70, 29.07 ± 9.45, and 31.24 ± 16.05 fold increase (FI) in current, respectively) compared to WT (25.89 ± 5.93 FI). In contrast, 500 nM SKA-121 activated the M368L mutant (66.55 ± 9.90 FI) more effectively than the WT channel. These results suggest that SKA-121 is probably siting somewhat differently in the $K_{Ca}3.1$ binding pocket than EBIO sits in the $K_{Ca}2.2$ binding pocket and is therefore not making contact with V365, which corresponds to A625 in $K_{Ca}2.3$ and A477 in $K_{Ca}2.2$. There instead seems to be an interaction with M368 (see Fig. 7). However, taken together with the $K_{Ca}2.3$ data above, the results strongly suggest that SKA-121 and SKA-31 bind at the CaM-BD/CaM interface similar to EBIO.

We next generated Rosetta homology models of the CaM-BD/CaM of $K_{Ca}2.3$ and $K_{Ca}3.1$ based on the $K_{Ca}2.2$ CaM-BD/CaM crystal structure (PDB ID: 4J9Z) (Zhang et al., 2013) and then used RosettaLigand computational modeling software to dock SKA-121 into the binding pocket formed at the CaM-BD/CaM interface as described in the Methods. The $K_{Ca}3.1$ model with the channel (green) and calmodulin (pink) in space filling representation with SKA-121 docked at the CaM-BD/CaM interface is shown in Figure 3A (pdb file provided in Data Supplement). We probed the model by mutating residues that were facing inwards into the putative binding pocket along a stretch of 11 amino acids (362 to 372 in $K_{Ca}3.1$) in the CaM-BD

of both $K_{Ca}2.3$ and $K_{Ca}3.1$ (Fig. 3B-D; pdb files provided in Data Supplement) and determined SKA-121 activity after first studying Ca^{2+} sensitivity of the mutants and excluding mutants not responding with nA currents to free intracellular Ca^{2+} concentrations of 3 μM. Overall, most mutations (Fig. 3C, 3D and 2C for $K_{Ca}3.1$) did not significantly change the response of $K_{Ca}2.3$ to 20 μM SKA-121 or of $K_{Ca}3.1$ to 500 nM SKA-121. The $K_{Ca}2.3$ mutants D623E and V629A, as well as the $K_{Ca}3.1$ mutants M368F and V365A/S367T/M368L were not functional even at saturating calcium concentrations and therefore could not be studied. As suggested by the models, substituting a conserved Ser facing into the binding pocket (S632 in $K_{Ca}2.3$ and S372 in $K_{Ca}3.1$) with an Arg made both $K_{Ca}2.3$ and $K_{Ca}3.1$ insensitive to SKA-121 (Fig. 3C and 3D). The only other interesting mutation was $K_{Ca}3.1$ R362S, which was significantly less sensitive to SKA-121 than WT $K_{Ca}3.1$ (Fig. 3D).

Mutational Confirmation of the K_{Ca} Activator Binding Pocket in $K_{Ca}3.1$. Since the most dramatic effect had been observed when mutating S372 in $K_{Ca}3.1$ to a charged and bulky Arg we hypothesized that this mutation would prevent activators from binding to the interface pocket and should render $K_{Ca}3.1$ generally insensitive to both benzimidazole-type activators like EBIO and NS309 as well as other napthothiazole/oxazole-type K_{Ca} activators like SKA-31 and SKA-111. Interestingly, the S372R mutation practically abolished sensitivity to SKA-31 (1 μM, Fig. 4A), SKA-111 (1 μM, Fig. 4B), and EBIO (100 μM, Fig. 4C) in comparison to the WT $K_{Ca}3.1$ channel, but did not significantly (P = 0.095) reduce the sensitivity of NS309 (1 μM, Fig. 4D). Rosetta models of the four compounds docked and energy minimized in CaM-BD/CaM of $K_{Ca}3.1$ were found to be in agreement with these observations. The lowest energy binding poses of SKA-111 (EC_{50} = 110 nM) and SKA-31 (EC_{50} = 260 nM) show two hydrogen bonds between the 2-position amino group and M51 and E54 in calmodulin, while E54 itself is part of an extensive hydrogen bond network including R362, E295 and N300 in $K_{Ca}3.1$ (Fig. 4A and

15

4B). The less potent EBIO only forms one hydrogen bond through its one available hydrogen bond donor on the imidazole nitrogen with the backbone carbonyl oxygen on M51 (Fig. 4C). NS309, which is the most potent $K_{Ca}3.1$ activator of all four compounds (EC_{50} ~30 nM) forms the same hydrogen bond with the backbone carbonyl oxygen on M51 through its indole NH but also extends its 3-position oxime group towards R362 and accepts a hydrogen bond from one of the NH_2 groups of the guanidine moiety of R362 (Fig. 4D).

R362 is a Key Residue for the Greater $K_{Ca}3.1$ Potency of SKA-121 and NS309. After thus confirming the general location of the napthothiazole/oxazole binding pocket we further investigated the $K_{Ca}3.1$ R362S mutation since this was the only one of our mutations that had selectively reduced SKA-121 potency on $K_{Ca}3.1$ (Fig. 3D). In order to understand this loss of potency we modeled the $K_{Ca}3.1$-R362S mutant and closely compared the lowest energy conformations of SKA-121 between WT-$K_{Ca}3.1$ (Fig. 5A, pdb provided in Data Supplement), $K_{Ca}3.1$-R362S (Fig. 5B) and WT-$K_{Ca}2.3$ (Fig. 5C; pdb provided in Data Supplement). In the WT-$K_{Ca}3.1$ model the amino group of SKA-121 forms hydrogen bonds with the backbone carbonyl oxygen on M51 and the side chain oxygen on E54 in calmodulin, while the E54 side chain oxygen itself is part of an extensive hydrogen bond network including R362, E295 and N300 in the $K_{Ca}3.1$ channel (Fig. 5A). If R362 in $K_{Ca}3.1$ is replaced by Ser like in the $K_{Ca}3.1$-R362S mutant (Fig. 5B), the two hydrogen bonds to M51 and E54 are still present in the majority of low energy binding poses, but the hydrogen bond network that involved R362 in the WT-$K_{Ca}3.1$ (Fig. 5A) is absent. Similarly, the $K_{Ca}2.3$ model is devoid of this hydrogen bond network (Fig. 5C). Full concentration response curves (Fig. 5D) revealed that the $K_{Ca}3.1$-R362S mutant is ~7-fold less sensitive to SKA-121 than the WT-$K_{Ca}3.1$ channel suggesting that R362 is one of the key residues responsible for the $K_{Ca}3.1$ selectivity of SKA-121, presumably because of its ability to stabilize E54 in CaM through a hydrogen bond network. In keeping with this idea, the $K_{Ca}3.1$-R362S mutant also significantly reduced the potency of SKA-31 and SKA-111 (Supplemental

Fig. 1). Conversely, the reverse mutation in $K_{Ca}2.3$, $K_{Ca}2.3$-S622R only slightly, but not significantly increased the sensitivity of $K_{Ca}2.3$ to SKA-121 (EC_{50} 8.75 μM versus 10.25 μM), suggesting that the presence of an Arg residue alone is not sufficient to generate a high affinity binding site for small molecule K_{Ca} activators in the $K_{Ca}2.3$-CaM-BD/CaM interface. Figure 6 shows an overlay of the lowest energy binding poses of NS309 (orange) and SKA-121 (dark green) illustrating that NS309 sits "more forward" in the CaM-BD/CaM interface of $K_{Ca}3.1$ than SKA-121 and forms a direct hydrogen bond with R362.

The $K_{Ca}3.1$ Selectivity of SKA-121 is Due to a Better Overall Hydrophobic Shape Complementarity. While the direct or indirect hydrogen bonding to R362 in $K_{Ca}3.1$ could thus be postulated to explain the greater $K_{Ca}3.1$ potency of both napthothiazole/oxazole-type K_{Ca} activators and NS309, this contact could still not explain the greater $K_{Ca}3.1$ selectivity of SKA-121 and SKA-111 when compared to their template SKA-31, since all three compounds, SKA-31 (Fig. 4A), SKA-111 (Fig. 4B) and SKA-121 (Fig. 5A) form two hydrogen bonds with M51 and E54 in calmodulin with a "background" stabilization of E54 from a hydrogen bond to R362. So in order to understand why the introduction of a methyl group in 5-position of the napthothiazole/oxazol ring system resulted in a roughly 2.5-fold gain in potency on $K_{Ca}3.1$ and a roughly 3-fold (SKA-121) drop in potency on $K_{Ca}2.3$ compared to SKA-31 (EC_{50} for $K_{Ca}2.3$ = 2.9 μM), we more closely scrutinized the hydrophobic protein ligand interactions in the CaM-BD/CaM interface for SKA-31 and SKA-121 in our Rosetta models (Fig. 7). The most prominent hydrophobic interactions formed by SKA-31 in the $K_{Ca}3.1$-CaM-BD/CaM interface involve the sulfur atom in its thiazole ring, which interacts with both M71 in CaM and V365 in $K_{Ca}3.1$ and the outer ring of the napthol system, which makes hydrophobic contacts with F19 and I63 in CaM and M368 in $K_{Ca}3.1$ (Fig. 7A). To experimentally confirm the interaction between the thiazole sulfur and V365 we tested SKA-31 on both the V365A and the V365F mutants and found that

17

V365A was roughly 2-fold more sensitive, while the V365F mutation, which had not affected

SKA-121 activity (Fig. 3) completely abolished SKA-31 but not NS309 activity (data not shown).

The remaining van der Waals interactions between the thiazole amino group of SKA-31 and

M51 and E54 further strengthen the above mentioned hydrogen bonds to these two CaM

residues (Fig. 7A). SKA-121 instead of contacting V365 and M71, only contacts M71 through its

oxazole nitrogen but "picks up" an additional contact with M51 through its oxazole oxygen and

three hydrophobic interactions between its 5-position methyl group and S372, M368 and M72

(Fig. 7C). A wire-mesh rendering of the surface area of SKA-121 in the $K_{Ca}3.1$-CaM-BD/CaM

interface pocket (Fig. 7B) illustrates a nearly perfect shape-complementarity between the $-CH_3$

group of SKA-121 and the pocket formed by S372, M368 and M72 in the channel/CaM

interface. SKA-31 in contrast does not fill this pocket as tightly, which could account for its ~2.5-

fold lower potency in activating $K_{Ca}3.1$ (Fig. 7D).

A detailed look at the hydrophobic interactions between SKA-31 and SKA-121 and the

$K_{Ca}2.3$-CaM-BD/CaM interface pocket reveal that both compounds make fewer hydrophobic

contacts (6 for SKA-31 and 5 for SKA-121) than in the $K_{Ca}3.1$ interface.

Discussion

K_{Ca} channels have a well-developed pharmacology in comparison to many other ion channels. $K_{Ca}2$ channels are blocked by the venom peptides apamin, scyllatoxin and tamapin and the bisquaternary small molecules UCL-1684 and UCL-1848 (Wulff et al., 2007). $K_{Ca}3.1$ channels in contrast are inhibited by the scorpion toxins maurotoxin (Castle et al., 2003) and charybdotoxin (Rauer et al., 2000), the triarylmethanes TRAM-34 (Wulff et al., 2000) and senicapoc (Stocker et al., 2003) as well as the benzothiazinone NS6180 (Strøbæk et al., 2013). In addition to these "simple" inhibitors, which either bind in the outer pore like the toxins or in the inner pore like the triarylmethanes and NS6180 (Nguyen et al., 2017), $K_{Ca}2/3$ channels also have positive and negative gating-modulators, which apparently render the channels more or less Ca^{2+}-sensitive by left-shifting or right-shifting the Ca^{2+}-response curve (Christophersen and Wulff, 2015). While negative gating modulators like NS8593 and (-)CM-TMPF interact with positions deep within the inner pore vestibule (Hougaard et al., 2012; Jenkins et al., 2011), where the gate of these channels is located (Bruening-Wright et al., 2007; Bruening-Wright et al., 2002), positive gating modulators had long been suspected to act through a site located in the C-terminal region, close to or at the CaM-BD based on work from Pedarzani *et al.*, who showed in 2001 that swapping of the C-terminus could transfer the higher EBIO sensitivity from $K_{Ca}3.1$ to $K_{Ca}2.2$ (Pedarzani et al., 2001). This prediction was more recently confirmed when Zhang *et al.* crystallized the $K_{Ca}2.2$ CaM-BD/CaM complex first with EBIO (Zhang et al., 2012) and then with NS309 (Zhang et al., 2013) in the interface of the CaM-BD and the CaM N-lobe. Since both EBIO and NS309 are unsuitable for *in vivo* experiments due to their low potency or metabolic instability, our group developed a series of $K_{Ca}2/3$ activators based on the more "drug-like" napthothiazole/oxazole scaffold (Coleman et al., 2014; Sankaranarayanan et al., 2009). Despite its much better pharmacokinetic properties, the first generation compound, SKA-31, only displayed a 7-fold selectivity for $K_{Ca}3.1$ over $K_{Ca}2$ channels, which is very similar to EBIO. In contrast, two of our

19

second generation compounds, SKA-121 and SKA-111, displayed greatly improved selectivity

for K_{Ca}3.1 over K_{Ca}2.3, which was caused by the introduction of a methyl group in 5-position of

the flat napthothiazole/oxazole ring system (Coleman et al., 2014).

We here set out to understand this "magic methyl" effect (Leung et al., 2012) at the

molecular level. Based on the overall structural similarity between SKA-31 and SKA-121 and

EBIO and NS309, we strongly suspected that napthothiazole/oxazole-type K_{Ca} activators are

also binding at the CaM-BD/CaM interface. However, since we had previously been totally

mistaken in the assumption that the negative gating modulator NS8593, which turned out to

have a binding site in the inner pore despite "looking" similar to EBIO and NS309 (Hougaard et

al., 2012; Jenkins et al., 2011), was binding at this interface, we first used site-directed

mutagenesis to confirm that this assumption was indeed valid. After localizing the binding site of

SKA-31 and SKA-121 to the K_{Ca} channel CaM-BD/CaM interface, we generated homology

models of the K_{Ca}3.1 and K_{Ca}2.3 CaM-BD/CaM complexes based on the crystal structure of the

K_{Ca}2.2 CaM-BD/CaM complex (Zhang et al., 2013) with the RosettaLigand computational

modeling software and then used these models to further guide experimentation to explore the

orientation of SKA-121 and other K_{Ca} activators in their binding pocket. Taken together, our

modeling and mutagenesis data suggest that all K_{Ca} activators (EBIO, NS309, SKA-31 and

SKA-121) hydrogen bond with CaM-M51 in both K_{Ca}3.1 and K_{Ca}2.3 channels. This hydrogen

bond is very likely also present in the K_{Ca}2.2 CaM-BD/CaM crystal structure (Zhang et al.,

2013)(pdb id: 4J9Z) where the hydrogen on the imidazole nitrogen of NS309 is in perfect

hydrogen bonding distance to the oxygen of the backbone carbonyl group of CaM-M51. The

more potent napthothiazole/oxazole-type K_{Ca} activators SKA-31, SKA-111 and SKA-121 (Fig. 4)

all from an additional second hydrogen bond with E54 and thus "anchor" themselves with their

2-position amino group on two carbonyl groups of the calmodulin N-lobe. This second hydrogen

bond is present in all our K_{Ca}3.1 and K_{Ca}2.3 docking models of K_{Ca} activators with an amino

group (see for example SKA-121 in K_{Ca}2.3 in Fig. 5C). What differentiates the most frequently

20

sampled lowest energy conformations of the $K_{Ca}3.1$ models with napthothiazole/oxazole-type K_{Ca} activators in the CaM-BD/CaM interface is the presence of an extensive hydrogen bond network with $K_{Ca}3.1$-R362 at its center that seems to stabilize CaM-E54 in an optimal position to hydrogen bond with the amino group of the docked ligand (Fig. 4 and Fig. 5). We therefore postulate that the presence of R362 in $K_{Ca}3.1$ is responsible for the generally observed 5-10-fold $K_{Ca}3.1$ selectivity of all K_{Ca} activators. NS309, the most potent $K_{Ca}3.1$ activator, directly hydrogen bonds with R362.

Having found a reasonable structural explanation in the presence of R362 for why $K_{Ca}3.1$ is more sensitive to SKA-31, SKA-121, SKA-111, and NS309 than $K_{Ca}2.3$, we next focused our attention on the CH_3 group in 5-position of the napthothiazole/oxazol ring system of SKA-121 and SKA-111. Interestingly, on closer inspection the effect of this group is not exactly what is classically termed the "magic methyl" effect (Leung et al., 2012), where the addition of a single methyl group in the "right" location on a scaffold results in a dramatic increase in activity, but rather a relatively modest 2.5-fold increase in potency on $K_{Ca}3.1$ combined with a moderate 3-5 loss in potency on $K_{Ca}2.3$ which overall results in a 40-100 fold increase in $K_{Ca}3.1$ selectivity compared with SKA-31. Given that these changes, although quite effective when combined, do not suggest major steric hindrance from stabilization of, for example, a large rotatable ring (Barreiro et al., 2011), we suspected that the gain in selectivity is primarily driven by hydrophobic interactions (e.g. the amount of hydrophobic protein surface buried upon ligand binding). The general magnitude of the so-called hydrophobic effects obtained from diverse sets of protein-ligand complexes for an additional methyl group is 30 cal/mol x Å^2 (Vallone et al., 1998), which is equivalent to a 3.5-fold increase in binding affinity (Bissantz et al., 2010) and roughly on the order of magnitude observed here for the increases and decreases in potency. A detailed examination of the van der Waals interactions in the lowest energy binding poses of SKA-121 and SKA-31 in our Rosetta models shows that both SKA-121 and SKA-31 make more hydrophobic contacts in the $K_{Ca}3.1$- than the $K_{Ca}2.3$-CaM-BD/CaM interface pocket. While "the

back" of both the $K_{Ca}3.1$ and the $K_{Ca}2.3$ interface is well "filled" by both compounds, actually so well that the presence of any water molecules or ions in the interface is highly unlikely after ligand binding, there is an overall greater shape complimentary between the lipophilic binding pocket formed by S372, M368 and M72 and the 5-position methyl group of SKA-121, which we postulate accounts for the gain in $K_{Ca}3.1$ selectivity observed with SKA-121.

Taken together we believe our current study provides an explanation for the generally greater potency of small molecule K_{Ca} channel activators like SKA-121 on $K_{Ca}3.1$ than $K_{Ca}2.3$. However, we were surprised by the variance in binding poses observed for SKA-31, its derivatives SKA-121 and SKA-111, EBIO and NS309. Depending on their substitution pattern and the heteroatoms present in their ring systems, the compounds twisted, turned, and shifted around in the CaM-BD/CaM interface pocket, and often underwent quite individualistic interactions with channel residues. While these findings are encouraging when considering the possibility of designing and identifying compounds with increased K_{Ca} channel subtype selectivity, they are also sobering and caution against transferring structure activity relationship findings between even closely related chemotypes without experimental data. Further structural, modeling and experimental studies will be needed to reveal the molecular mechanisms of action of small molecule K_{Ca} channel activators in the full-length K_{Ca} channel structures.

Authorship Contributions

Participated in research design: Brandon M. Brown, Heesung Shim, Vladimir Yarov-Yarovoy, Miao Zhang, Heike Wulff

Conducted patch-clamp recordings and data analysis: Brandon M. Brown

Performed molecular modeling and related data analysis: Heesung Shim, Vladimir Yarov-Yarovoy

Wrote or contributed to the writing of the manuscript: Brandon M. Brown, Heesung Shim, Miao Zhang, Vladimir Yarov-Yarovoy, Heike Wulff

References

Adelman JP, Maylie J and Sah P (2012) Small-conductance Ca^{2+}-activated K^+ channels: form and function. *Ann Rev Physiol* **74**:245-269.

Barreiro EJ, Kummerle AE and Fraga CA (2011) The methylation effect in medicinal chemistry. *Chem Rev* **111**:5215-5246.

Barth P, Schonbrun J and Baker D (2007) Toward high-resolution prediction and design of transmembrane helical protein structures. *Proc Natl Acad Sci USA* **104**:15682-15687.

Bissantz C, Kuhn B and Stahl M (2010) A medicinal chemist's guide to molecular interactions. *J Med Chem* **53**:5061-5084.

Bonneau R, Strauss CE, Rohl CA, Chivian D, Bradley P, Malmstrom L, Robertson T and Baker D (2002) De novo prediction of three-dimensional structures for major protein families. *J Mol Biol* **322**:65-78.

Bruening-Wright A, Lee WS, Adelman JP and Maylie J (2007) Evidence for a deep pore activation gate in small conductance Ca^{2+}-activated K^+ channels. *J Gen Physiol* **130**:601-610.

Bruening-Wright A, Schumacher MA, Adelman JP and Maylie J (2002) Localization of the activation gate for small conductance Ca^{2+}-activated K^+ channels. *J Neurosci* **22**:6499-6506.

Busse R, Edwards G, Feletou M, Fleming I, Vanhoutte PM and Weston AH (2002) EDHF: bringing the concepts together. *Trends Pharmacol Sci* **23**:374-380.

Cao Y, Dreixler JC, Roizen JD, Roberts MT and Houamed KM (2001) Modulation of recombinant small-conductance Ca²⁺-activated K⁺ channels by the muscle relaxant chlorzoxazone and structurally related compounds. *J Pharmacol Exp Ther* **296**:683-689.

Castle NA, Lodon DO, Creech C, Fajloun Z, Stocker JW and Sabatier J-M (2003) Maurotoxin - a potent inhibitor of the intermediate conductance Ca²⁺-activated potassium channel. *Mol Pharmacol* **63**:409-418.

Chandy KG, Fantino E, Wittekindt O, Kalman K, Tong LL, Ho TH, Gutman GA, Crocq MA, Ganguli R, Nimgaonkar V, Morris-Rosendahl DJ and Gargus JJ (1998) Isolation of a novel potassium channel gene hSKCa3 containing a polymorphic CAG repeat: a candidate for schizophrenia and bipolar disorder? *Mol Psychiatry* **3**:32-37.

Christophersen P and Wulff H (2015) Pharmacological gating modulation of small- and intermediate-conductance Ca-activated K channels (K2.x and K3.1). *Channels (Austin)*:1-8.

Coleman N, Brown BM, Olivan-Viguera A, Singh V, Olmstead MM, Valero MS, Köhler R and Wulff H (2014) New positive Ca²⁺-activated K⁺ channel gating modulators with selectivity for KCa3.1. *Mol Pharmacol* **86**:342-357.

Davis IW and Baker D (2009) RosettaLigand docking with full ligand and receptor flexibility. *J Mol Biol* **385**:381-392.

Davis IW, Raha K, Head MS and Baker D (2009) Blind docking of pharmaceutically relevant compounds using RosettaLigand. *Protein Sci* **18**:1998-2002.

Devor DC, Singh AK, Frizzell RA and Bridges RJ (1996) Modulation of Cl$^-$ secretion by benzimidazolones. I. Direct activation of a Ca^{2+}-dependent K$^+$ channel. *Am J Physiol* **271**:L775-784.

Fanger CM, Ghanshani S, Logsdon NJ, Rauer H, Kalman K, Zhou J, Beckingham K, Chandy KG, Cahalan MD and Aiyar J (1999) Calmodulin mediates calcium-dependent activation of the intermediate conductance KCa channel, IKCa1. *J Biol Chem* **274**:5746-5754.

Feske S, Wulff H and Skolnik EY (2015) Ion channels in innate and adaptive immunity. *Ann Rev Immunol* **33**:291-353.

Gerlach AC, Syme CA, Giltinan L, Adelman JP and Devors DC (2001) ATP-dependent activation of the intermediate conductance, Ca^{2+}-activated K$^+$ channel, hIK1, is conferred by a C-terminal domain. *J Biol Chem* **276**:10963-10970.

Hawkins PC and Nicholls A (2012) Conformer generation with OMEGA: learning from the data set and the analysis of failures. *J Chem Inf Model* **52**:2919-2936.

Hawkins PC, Skillman AG, Warren GL, Ellingson BA and Stahl MT (2010) Conformer generation with OMEGA: algorithm and validation using high quality structures from the Protein Databank and Cambridge Structural Database. *J Chem Inf Model* **50**:572-584.

Hougaard C, Eriksen BL, Jorgensen S, Johansen TH, Dyhring T, Madsen LS, Strøbæk D and Christophersen P (2007) Selective positive modulation of the SK3 and SK2 subtypes of small conductance Ca^{2+}-activated K$^+$ channels. *Br J Pharmacol* **151**:655-665.

Hougaard C, Hammami S, Eriksen BL, Sorensen US, Jensen ML, Strøbæk D and Christophersen P (2012) Evidence for a common pharmacological interaction site on K(Ca)2 channels providing both selective activation and selective inhibition of the human K(Ca)2.1 subtype. *Mol Pharmacol* **81**:210-219.

Jenkins DP, Strøbæk D, Hougaard C, Jensen ML, Hummel R, Sorensen US, Christophersen P and Wulff H (2011) Negative gating modulation by (R)-*N*-(benzimidazol-2-yl)-1,2,3,4-tetrahydro-1-naphthylamine (NS8593) depends on residues in the inner pore vestibule: pharmacological evidence of deep-pore gating of KCa2 channels. *Mol Pharmacol* **79**:899-909.

Jensen BS, Strøbæk D, Christophersen P, Jorgensen TD, Hansen C, Silahtaroglu A, Olesen SP and Ahring PK (1998) Characterization of the cloned human intermediate-conductance Ca^{2+}-activated K^+ channel. *Am J Physiol* **275**:C848-856.

Jones HM, Bailey MA, Baty CJ, Macgregor GG, Syme CA, Hamilton KL and Devor DC (2007) An NH2-terminal multi-basic RKR motif is required for the ATP-dependent regulation of hIK1. *Channels (Austin)* **1**:80-91.

Lam J, Coleman N, Garing AL and Wulff H (2013) The therapeutic potential of small-conductance KCa2 channels in neurodegenerative and psychiatric diseases. *Expert Opin Ther Targets* **17**:1203-1220.

Lappin SC, Dale TJ, Brown JT, Trezise DJ and Davies CH (2005) Activation of SK channels inhibits epileptiform bursting in hippocampal CA3 neurons. *Brain Res* **1065**:37-46.

MOL #10941

Leung CS, Leung SS, Tirado-Rives J and Jorgensen WL (2012) Methyl effects on protein-ligand binding. *J Med Chem* **55**:4489-4500.

Li W, Halling DB, Hall AW and Aldrich RW (2009) EF hands at the N-lobe of calmodulin are required for both SK channel gating and stable SK-calmodulin interaction. *J Gen Physiol* **134**:281-293.

Logsdon NJ, Kang J, Togo JA, Christian EP and Aiyar J (1997) A novel gene, hKCa4, encodes the calcium-activated potassium channel in human T lymphocytes. *J Biol Chem* **272**:32723-32726.

Mandell DJ, Coutsias EA and Kortemme T (2009) Sub-angstrom accuracy in protein loop reconstruction by robotics-inspired conformational sampling. *Nat Methods* **6**:551-552.

Meiler J and Baker D (2006) ROSETTALIGAND: protein-small molecule docking with full side-chain flexibility. *Proteins* **65**:538-548.

Nguyen HM, Singh V, Pressly B, Jenkins DP, Wulff H and Yarov-Yarovoy V (2017) Structural insights into the atomistic mechanisms of action of small molecule inhibitors targeting the KCa3.1 channel pore. *Mol Pharmacol* **91**:392-402.

OEChem v OpenEye Scientific Software, Inc. *http://wwweyesopencom Santa Fe, NM, USA*.

Pedarzani P, Mosbacher J, Rivard A, Cingolani LA, Oliver D, Stocker M, Adelman JP and Fakler B (2001) Control of electrical activity in central neurons by modulating the gating of small conductance Ca^{2+}-activated K^+ channels. *J Biol Chem* **276**:9762-9769.

28

Pettersen EF, Goddard TD, Huang CC, Couch GS, Greenblatt DM, Meng EC and Ferrin TE (2004) UCSF Chimera--a visualization system for exploratory research and analysis. *J Comput Chem* **25**:1605-1612.

Rauer H, Lanigan MD, Pennington MW, Aiyar J, Ghanshani S, Cahalan MD, Norton RS and Chandy KG (2000) Structure-guided transformation of charybdotoxin yields an analog that selectively targets Ca^{2+}-activated over voltage-gated K^+ channels. *J Biol Chem* **275**:1201-1208.

Rohl CA, Strauss CE, Misura KM and Baker D (2004) Protein structure prediction using Rosetta. *Methods Enzymol* **383**:66-93.

Sankaranarayanan A, Raman G, Busch C, Schultz T, Zimin PI, Hoyer J, Kohler R and Wulff H (2009) Naphtho[1,2-*d*]thiazol-2-ylamine (SKA-31), a new activator of KCa2 and KCa3.1 potassium channels, potentiates the endothelium-derived hyperpolarizing factor response and lowers blood pressure. *Mol Pharmacol* **75**:281-295.

Singh S, Syme CA, Singh AK, Devor DC and Bridges RJ (2001) Benzimidazolone activators of chloride secretion: potential therapeutics for cystic fibrosis and chronic obstructive pulmonary disease. *J Pharmacol Exp Ther* **296**:600-611.

Stocker JW, De Franceschi L, McNaughton-Smith GA, Corrocher R, Beuzard Y and Brugnara C (2003) ICA-17043, a novel Gardos channel blocker, prevents sickled red blood cell dehydration in vitro and in vivo in SAD mice. *Blood* **101**:2412-2418.

Strøbæk D, Brown DT, Jenkins DP, Chen YJ, Coleman N, Ando Y, Chiu P, Jorgensen S, Demnitz J, Wulff H and Christophersen P (2013) NS6180, a new KCa3.1 channel inhibitor prevents T-cell activation and inflammation in a rat model of inflammatory bowel disease. *Br J Pharmacol* **168**:432-444.

Syme CA, Gerlach AC, Singh AK and Devor DC (2000) Pharmacological activation of cloned intermediate- and small-conductance Ca^{2+}-activated K^+ channels. *Am J Physiol Cell Physiol* **278**:C570-581.

Vallone B, Miele AE, Vecchini P, Chiancone E and Brunori M (1998) Free energy of burying hydrophobic residues in the interface between protein subunits. *Proc Natl Acad Sci USA* **95**:6103-6107.

Wang C, Bradley P and Baker D (2007) Protein-protein docking with backbone flexibility. *J Mol Biol* **373**:503-519.

Wei AD, Gutman GA, Aldrich R, Chandy KG, Grissmer S and Wulff H (2005) International Union of Pharmacology. LII. Nomenclature and molecular relationships of calcium-activated potassium channels. *Pharmacol Rev* **57**:463-472.

Wulff H and Castle NA (2010) Therapeutic potential of KCa3.1 blockers: recent advances and promising trends. *Expert Rev Clin Pharmacol* **3**:385-396.

Wulff H, Gutman GA, Cahalan MD and Chandy KG (2001) Delination of the clotrimazole/TRAM-34 binding site on the intermediate conductance calcium-activated potassium channel IKCa1. *J Biol Chem* **276**:32040-32045.

Wulff H, Kolski-Andreaco A, Sankaranarayanan A, Sabatier JM and Shakkottai V (2007) Modulators of small- and intermediate-conductance calcium-activated potassium channels and their therapeutic indications. *Cur Med Chem* **14**:1437-1457.

Wulff H, Miller MJ, Haensel W, Grissmer S, Cahalan MD and Chandy KG (2000) Design of a potent and selective inhibitor of the intermediate-conductance Ca^{2+}-activated K^+ channel, IKCa1: A potential immunosuppressant. *Proc Natl Acad Sci USA* **97**:8151-8156.

Xia XM, Fakler B, Rivard A, Wayman G, Johnson-Pais T, Keen JE, Ishii T, Hirschberg B, Bond CT, Lutsenko S, Maylie J and Adelman JP (1998) Mechanism of calcium gating in small-conductance calcium-activated potassium channels. *Nature* **395**:503-507.

Yarov-Yarovoy V, Schonbrun J and Baker D (2006) Multipass membrane protein structure prediction using Rosetta. *Proteins* **62**:1010-1025.

Zhang M, Pascal JM, Schumann M, Armen RS and Zhang JF (2012) Identification of the functional binding pocket for compounds targeting small-conductance Ca^{2+}-activated potassium channels. *Nature Communications* **3**:1021.

Zhang M, Pascal JM and Zhang JF (2013) Unstructured to structured transition of an intrinsically disordered protein peptide in coupling Ca^{2+}-sensing and SK channel activation. *Proc Natl Acad Sci USA* **110**:4828-4833.

Footnotes

Address of persons to receive reprint requests:

Heike Wulff, Department of Pharmacology, Genome and Biomedical Sciences Facility, Room 3502, 451 Health Sciences Drive, University of California, Davis, Davis, CA 95616; phone: 530-754-6136; email: hwulff@ucdavis.edu

Figure Legends

Fig. 1. SKA-121 displays 40-fold selectivity for $K_{Ca}3.1$ over $K_{Ca}2.3$ but is a positive gating modulator for both channels. (A) Whole-cell $K_{Ca}3.1$ current with an intracellular free calcium concentration of 250 nM in the presence and absence of 1 µM SKA-121. (B) Whole-cell $K_{Ca}2.3$ current with an intracellular free calcium concentration of 500 nM in the presence and absence of 1 µM SKA-121. Both traces in A and B were elicited by voltage ramps from -120 to + 40 mV applied every 10 sec. *Inside-out K_{Ca} channel experiments.* (C) Calcium concentration response curves for $K_{Ca}3.1$ in the presence (EC_{50} = 424 nM, 95% CI: 399–454 nM, n_H = 3.1) and absence (EC_{50} = 590 nM, 95% CI: 556-625 nM, n_H = 2.9) of 500 nM SKA-121. (D) Calcium concentration response curves for $K_{Ca}2.3$ in the presence (EC_{50} = 406 nM, 95% CI: 318 -518 nM, n_H = 2.2) and absence (EC_{50} = 1.189 µM, 95% CI: 0.999-1.904 nM, n_H = 2.7) of 20 µM SKA-121. Data points are mean ± SD; n = 3-5 independent cells/data point. An extra sum-of-squares F test (GraphPad Prism5) to compare the curves rendered *P* values of < 0.0001 for the comparison of both the $K_{Ca}3.1$ and the $K_{Ca}2.3$ calcium sensitivity in the presence and absence of SKA-121.

Fig. 2. (A) Sequence alignment of the calcium-binding domain of $K_{Ca}2.2$, $K_{Ca}2.3$, and $K_{Ca}3.1$. Zhang *et al.* mutated the highlighted residues in $K_{Ca}2.2$, A to V and L to M, to the corresponding $K_{Ca}3.1$ residues and demonstrated increased EBIO sensitivity. (B) Responses of the $K_{Ca}2.3$-CaMBD mutants A625V/L628M and A625I to SKA-31. While SKA-31 at a concentration of 1 µM does not elicit an increase in current for all three channels, 5 and 10 µM of SKA-31 produce strong current increases in the WT-$K_{Ca}2.3$ channel that are significantly reduced in both the A625V/L628M and A625I-$K_{Ca}2.3$ mutants. (C) Summary of the initial $K_{Ca}3.1$ whole-cell experiments in response to SKA-121. Position V365 does not appear to be involved in SKA-121

binding since current increases in response to 500 nM SKA-121 compared to WT-K_{Ca}3.1 are not statistically different for both the V365A and V365F mutants. The M368L mutant in contrast displays an increased current response to 500 nM SKA-121 (P = 4.076E^{-4}), suggesting that M368 is involved in SKA-121 binding. All values are mean ± S.D. n = 5-8 cells per mutant channel (two sample t-test assuming equal variance). * = P < 0.05, ** = P < 0.01, *** = P < 0.001.

Fig. 3. (A) Space fill rendering of the Rosetta model of SKA-121 docked into the interface between the K_{Ca}3.1 CaM-BD (light green) and CaM (pink). (B) Sequence alignment of the CaM-BD of K_{Ca}3.1 and K_{Ca}2.3. (C) Effect of K_{Ca}2.3 mutations on the current activating effect of 20 μM SKA-121. Shown are fold increases in comparison to control currents elicited by 500 nM free internal Ca^{2+}. (D) Effect of K_{Ca}3.1 mutations on the current activating effect of 500 nM SKA-121. Shown are fold increases in comparison to control currents elicited by 250 nM free internal Ca^{2+}. Shown are mean ± S.D.; n = 5-8 cells per mutant (two sample t-test assuming equal variance). * = P < 0.05, ** = P < 0.01, *** = P < 0.001.

Fig. 4. The K_{Ca}3.1-S372R mutation significantly reduces the potency of SKA-31 (A, P = 0.024), SKA-111 (B, P = 0.004) and EBIO (C, P = 0.0002), but not NS309 (D, P = 0.095). Shown are fold increases in current (mean ± SD) compared to WT control at 250 nM free internal [Ca^{2+}] from = 3-6 independent cells per condition (two sample t-test assuming equal variance). * = P < 0.05, ** = P < 0.01, *** = P < 0.001.

Fig. 5. Rosetta models of the lowest energy binding poses of SKA-121 in the interface between CaM (pink) and the CaM-BD (light green) of WT-K_{Ca}3.1 (A), the K_{Ca}3.1-R362S mutant (B), and WT-K_{Ca}2.3 (C). (D) Concentration-response curves for SKA-121 induced current activation: WT-K_{Ca}3.1 (EC$_{50}$ = 128 nM, 95% CI: 84-194 nM, n_H = 1.3), K_{Ca}3.1-R362S (EC$_{50}$ = 851 nM, 95% CI:

0.662-1.288 μM, n_H = 1.3), K_{Ca}2.3-A625V (EC$_{50}$ = 4.73 μM, 95% CI: 2.84-5.72 μM, n_H = 2.8), K_{Ca}2.3-S622R (EC$_{50}$ = 8.45 μM, 95% CI: 7.42-9.55 μM, n_H = 2.8), WT-K_{Ca}2.3 (EC$_{50}$ = 10.25 μM, 95% CI: 6.16-33.59 μM, n_H = 2.7). Data points are expressed as mean ± SD; n = 3-5 independent cells/data point. An extra sum-of-squares F test (GraphPad Prism5) to compare the curves rendered a P value < 0.0001 for the comparison betweeb WT-K_{Ca}3.1 and the K_{Ca}3.1-R362S mutant. Comparisons of the K_{Ca}2.3 mutants to WT-K_{Ca}2.3 showed that the SKA-121 EC$_{50}$ was significantly different for the K_{Ca}2.3-A625V (P = 0.0091) but not the K_{Ca}2.3-S622R (P = 0.6636) mutant.

Fig. 6. Overlay of the lowest energy binding poses of NS309 (orange) and SKA-121 (dark green) in the interface between the K_{Ca}3.1-CaM-BD (light green) and CaM (pink). While R362 in K_{Ca}3.1 does not directly interact with SKA-121, it stabilizes E54 in CaM through three hydrogen bonds. NS309 in contrast "sits more forward" and is stabilized through a direct hydrogen bond with R362 and M51. The inset on the right shows an overlay of NS309 and SKA-121 with all channel residues removed for clarity.

Fig. 7. Hydrophobic interactions (dark purple) in the lowest energy binding poses of SKA-31 (A) and SKA-121 (B) in the K_{Ca}3.1-CaM-BD/CaM interface. K_{Ca}3.1 (light green) or CaM (pink) residues within a 5 Å radius of the ligand undergoing hydrophobic interactions are shown explicitly in a stick rendering. Residues not forming interactions are hidden for clarity. The hydrogen bonds to M51 and E54 in CaM are also not shown for clarity. Wire-mesh rendering of the surface area of SKA-31 (B) and SKA-121 (D) in the K_{Ca}3.1-CaM-BD/CaM interface pocket viewed from the same angle as in panel A and B. (E,F) Hydrophobic interactions (dark purple) in the lowest energy binding poses of SKA-31 (E) and SKA-121 (F) in the K_{Ca}2.3-CaM-BD/CaM interface.
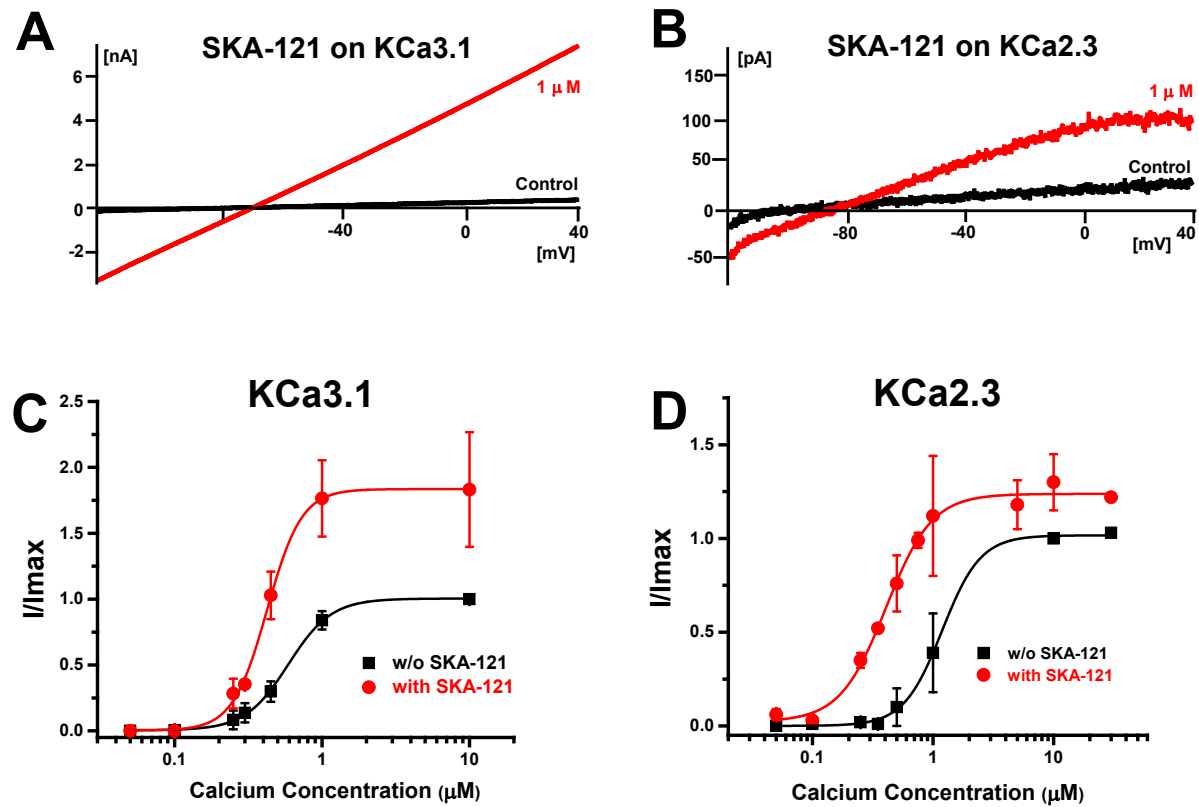
Figure 1

A

EBIO binding
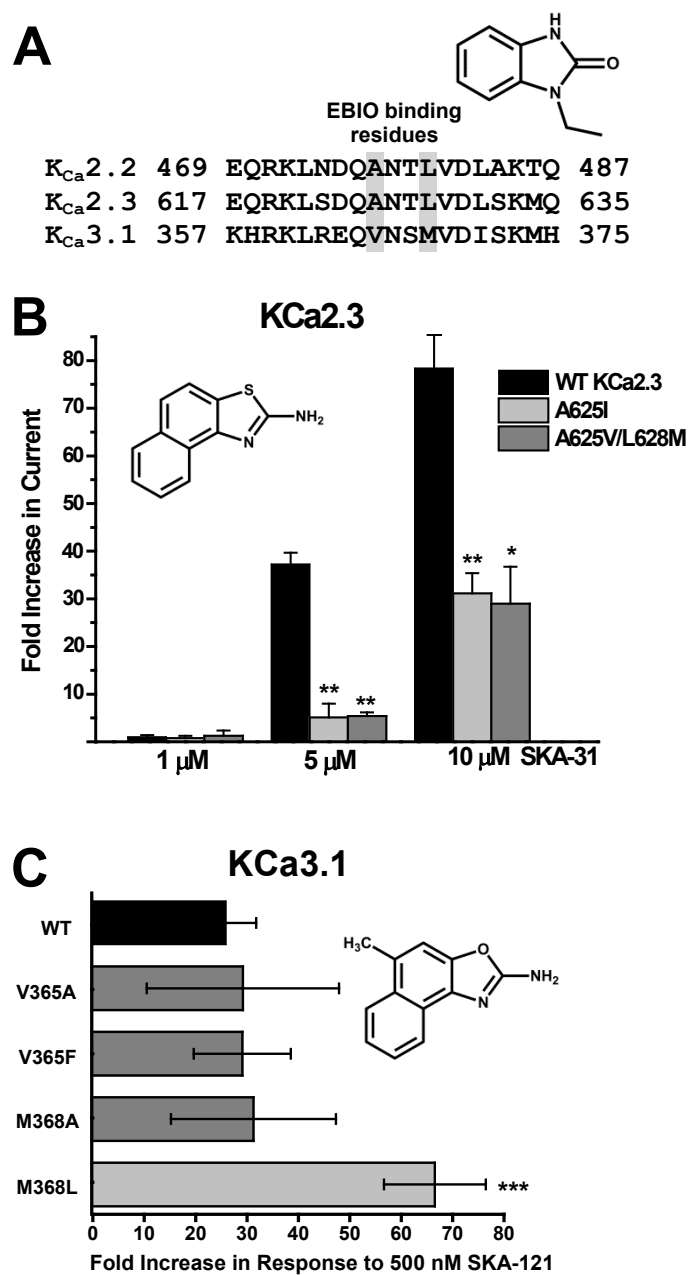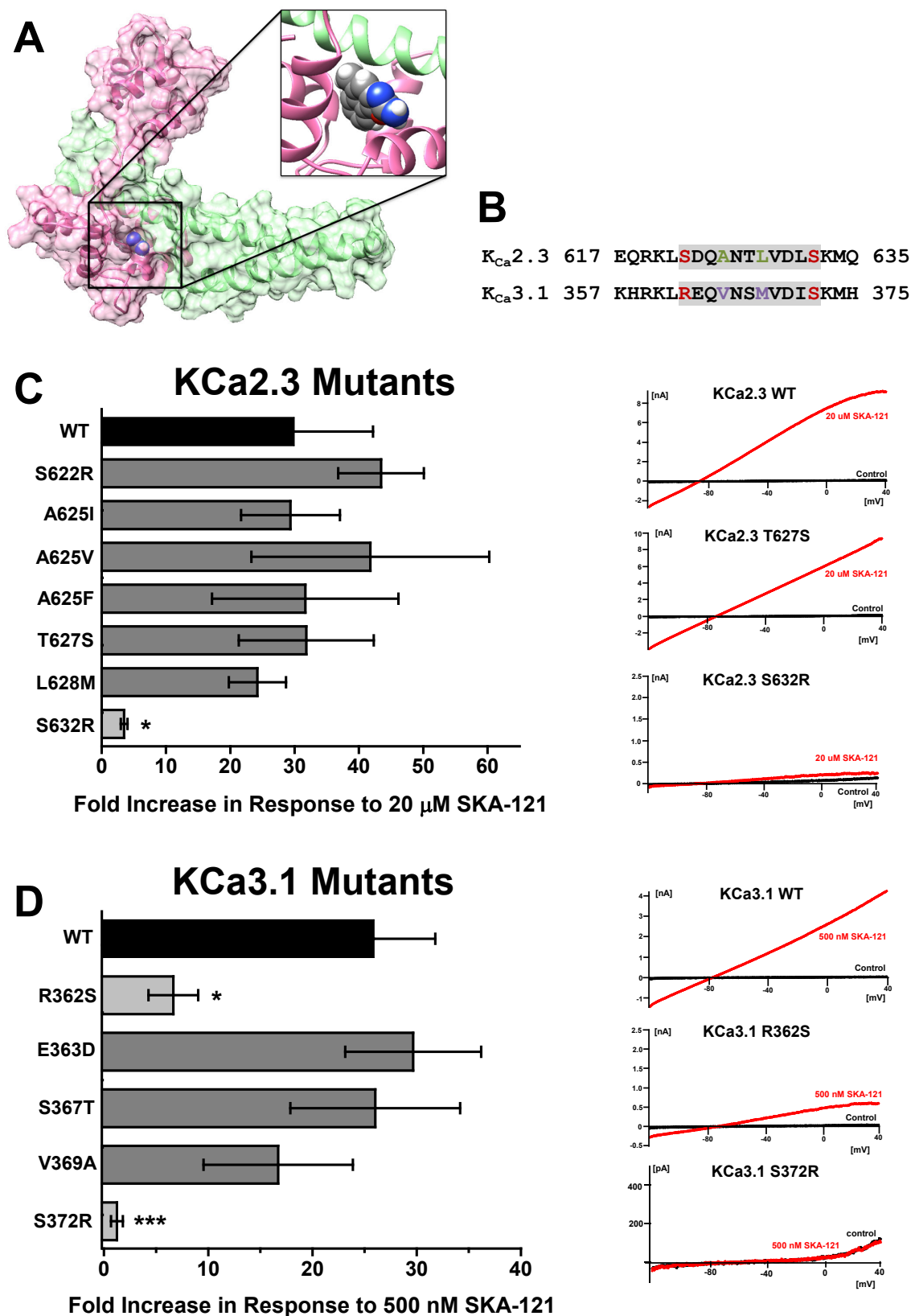residues

K_{Ca}2.2 469 EQRKLNDQANTLVDLAKTQ 487
K_{Ca}2.3 617 EQRKLSDQANTLVDLSKMQ 635
K_{Ca}3.1 357 KHRKLREQVNSMVDISKMH 375

B

C

Figure 2

A

B

K$_{Ca}$2.3 617 EQRKL**S**DQ**A**NT**L**VDL**S**KMQ 635

K$_{Ca}$3.1 357 KHRKL**R**EQ**V**NS**M**VDI**S**KMH 375

C **KCa2.3 Mutants**

Fold Increase in Response to 20 μM SKA-121

KCa2.3 WT
20 uM SKA-121
Control

KCa2.3 T627S
20 uM SKA-121
Control

KCa2.3 S632R
20 uM SKA-121
Control

D **KCa3.1 Mutants**

Fold Increase in Response to 500 nM SKA-121

KCa3.1 WT
500 nM SKA-121
Control

KCa3.1 R362S
500 nM SKA-121
Control

KCa3.1 S372R
control
500 nM SKA-121

Figure 3

Figure 4

Figure 5

Figure 6

Figure 7